Viscoplastic Selfconsistent Modelling of the Anisotropic Behavior of Voided Polycrystals

Ricardo A. Lebensohn, Paul J. Maudlin, and Carlos N. Tomé

Los Alamos National Laboratory, Los Alamos, NM 87545, USA

Abstract. In this work we consider the presence of ellipsoidal voids inside polycrystals submitted to large strain deformation. For this purpose, the originally incompressible viscoplastic selfconsistent (VPSC) formulation has been extended to deal with compressible polycrystals. Such an extended model allows us to account for porosity evolution in voided polycrystals, while preserving the anisotropy and crystallographic capabilities of the VPSC formulation. We present several applications of this extended VPSC model, which address the coupling between texture, plastic anisotropy, void shape, triaxiality, and porosity evolution. We also discuss the implementation of a multiscale calculation using the present compressible VPSC as constitutive routine inside dynamic FEM codes, for the simulation of deformation processes in which both anisotropy and cavitation become relevant aspects of microstructural evolution.

INTRODUCTION

The evolution of porosity is of relevance for assessing damage during both quasi-static and high-strain-rate deformation of metallic aggregates. The Gurson criterion [1], which provides a constitutive description of yield stress and porosity evolution, is widely used in simulations of metal deformation. The Gurson model is based on a number of simple assumptions (isotropic behavior of the matrix material, spherical voids, and rate independence). Such assumptions do not adequately represent many situations in which the anisotropy associated with void shape and material properties and/or rate effects may play a role. In this work we present a 3D viscoplastic selfconsistent (VPSC) model for polycrystal with prexisiting voids, which allows consideration of the full anisotropy associated with morphologic evolution of voids and grains and with crystallographic texture development in the aggregate, as well as rate effects. This formulation is a generalization of the tangent incompressible fully anisotropic VPSC formulation developed by Lebensohn and Tomé [2]. This model treated each grain as a viscoplastic ellipsoidal inclusion embedded in a Homogeneous Effective Medium (HEM). Both, the inclusion and the HEM were anisotropic and incompressible. As a consequence, the model was formulated in the deviatoric 5-dim space. In the present extension, cavities are also assumed to be ellipsoidal inclusions, but the assumption of incompressibility does not apply neither to the pores nor to the HEM (the inclusions representing grains, however, remain incompressible). Dilatation and hydrostatic pressure have to be accounted for and represent now the sixth dimension of the problem.

In what follows, we present a compact description of the formalism, and then illustrate some of the capabilities of the model. A full derivation of the formulation can be found elsewhere [3,4].

MODEL

The deviatoric part of the constitutive behavior of the material at local level is described by means of the non-linear rate-sensitivity equation:

$$\dot{\varepsilon}'_{ij}(\bar{x}) = \dot{\gamma}_o \sum_s m^s_{ij} \left(\frac{m^s_{kl} : \sigma'_{kl}(\bar{x})}{\tau^s} \right)^n \qquad (1)$$

where $\dot{\varepsilon}'(\bar{x})$ and $\sigma'(\bar{x})$ are the deviatoric strain-rate and stress fields; m^s_{ij} and τ^s are the Schmid

CP712, *Materials Processing and Design: Modeling, Simulation and Applications,* NUMIFORM 2004,
edited by S. Ghosh, J. C. Castro, and J. K. Lee

tensor and the threshold stress of slip (s); $\dot{\gamma}_o$ is a normalization factor and n is the rate-sensitivity exponent. Linearizing (1) inside the domain of a grain and adding the spherical local relation gives:

$$\left| \begin{array}{l} \dot{\varepsilon}'_{ij} = M_{ijkl}\,\sigma'_{kl} + \dot{\varepsilon}'^{o}_{ij} \\ \dot{\varepsilon}_{kk} = p/K \end{array} \right. \tag{2}$$

where $\dot{\varepsilon}'$ and σ' are the average local quantities in the grains; M_{ijkl} and $\dot{\varepsilon}'^{o}_{ij}$ are the local compliance and the back extrapolated term and $\dot{\varepsilon}_{kk}$, p and K are average local dilatation-rate, pressure and viscoplastic bulk modulus, respectively. M_{ijkl} and $\dot{\varepsilon}'^{o}_{ij}$ can be chosen differently. The best choice of them for the case of voided polycrystals is discussed later in this section. Performing homogenization consists in assuming a constitutive relation analogous to (2) at polycrystal level:

$$\left| \begin{array}{l} \dot{E}'_{ij} = \overline{M}_{ijkl}\,\Sigma'_{kl} + \dot{E}'^{o}_{ij} \\ \dot{E}_{kk} = P/\overline{K} \end{array} \right. \tag{3}$$

where, by comparison with (2), the meaning of the macroscopic state variables and moduli becomes aparent. Using the equivalent inclusion method the local (heterogeneous) constitutive behavior can be rewritten in terms of the (homogeneous) macroscopic moduli as:

$$\left| \begin{array}{l} \dot{\varepsilon}'_{ij} = \overline{M}_{ijkl}\,\sigma'_{kl} + \dot{E}'^{o}_{ij} + \dot{\varepsilon}^{*}_{ij} \\ \dot{\varepsilon}_{kk} = p/\overline{K} + \dot{\varepsilon}^{\#} \end{array} \right. \tag{4}$$

where $\dot{\varepsilon}^{*}_{ij}$ and $\dot{\varepsilon}^{\#}$ are the deviatoric eigen-strain-rate and a newly defined eigen-dilatation-rate, respectively. Rearranging and subtracting (3) from (4) gives:

$$\left| \begin{array}{l} \tilde{\sigma}'_{ij} = \overline{L}_{ijkl}\left(\tilde{\dot{\varepsilon}}'_{kl} - \dot{\varepsilon}^{*}_{kl}\right) \\ \tilde{p} = \overline{K}\left(\tilde{\dot{\varepsilon}}_{kk} - \dot{\varepsilon}^{\#}\right) \end{array} \right. \tag{5}$$

where the "~" quantities are local deviations from macroscopic values and $\overline{L}_{ijkl} = \overline{M}^{-1}_{ijkl}$. Using the equilibrium condition: $\sigma_{ij,j} = \tilde{\sigma}_{ij,j} = \tilde{\sigma}'_{ij,j} - \tilde{p}_{,i}$ and having in mind the relation between strain-rate and velocity-gradient, i.e.: $\tilde{\dot{\varepsilon}}_{ij} = \frac{1}{2}\left(\tilde{\dot{u}}_{i,j} + \tilde{\dot{u}}_{j,i}\right)$, gives:

$$\left| \begin{array}{l} \overline{L}_{ijkl}\,\tilde{\dot{u}}_{k,lj} + \tilde{p}_{,i} + f_i = 0 \\ \overline{K}\,\tilde{\dot{u}}_{k,k} - \tilde{p} + F = 0 \end{array} \right. \tag{6}$$

where the heterogeneity terms are: $f_i = -\overline{L}_{ijkl}\dot{\varepsilon}^{*}_{kl,j}$ and $F = -\overline{K}\dot{\varepsilon}^{\#}$. Equation (6) represents a system of 4 differential equations with 4 unknowns (3 components of the deviation in velocity $\tilde{\dot{u}}_i$ and one deviation in hydrostatic pressure $\tilde{p}$). After solving these differential equations using Green functions and Fourier transforms [3,4] we obtain:

$$\left| \begin{array}{l} \tilde{\dot{\varepsilon}}'_{ij} = S_{ijmn}\dot{\varepsilon}^{*}_{mn} + \beta_{ij}\,\tilde{\dot{\varepsilon}}_{kk} \\ \tilde{\dot{\varepsilon}}_{kk} = S_{kkmn}\dot{\varepsilon}^{*}_{mn} + \Psi\ \dot{\varepsilon}^{\#} \end{array} \right. \tag{7}$$

where S_{ijkl} is the fourth order viscoplastic deviatoric Eshelby tensor, $\Psi = S^{s}_{kk}$ (Ψ and S^{s}_{ij} are the newly defined viscoplastic spherical Eshelby factor and tensor, respectively) and $\beta_{ij} = S^{s}_{ij}/\Psi - \frac{1}{3}\delta_{ij}$ is a tensor that vanishes if the medium is isotropic. Inverting (7) and replacing in (5) we obtain the interaction equations:

$$\left| \begin{array}{l} \tilde{\dot{\varepsilon}}'_{ij} = -\tilde{M}_{ijkl}\,\tilde{\sigma}'_{kl} - \tilde{\beta}_{kl} \\ \tilde{\dot{\varepsilon}}_{kk} = -\tilde{p}/\tilde{K} \end{array} \right. \tag{8}$$

where $\tilde{M} = (I - S) : S^{-1} : \overline{M}$; $\tilde{\beta} = -S^{-1} : \beta\ \tilde{\dot{\varepsilon}}_{kk}$ and $\tilde{K} = (1 - \Psi)\Psi^{-1}\overline{K}$. Replacing the constitutive relations (2) and (3) in (8) gives the following self-consistent equations for the macroscopic moduli:

$$\overline{M} = \langle B \rangle^{-1} : \langle M : B \rangle \tag{9}$$

$$\dot{E}'^{o} = \left\langle M : \Phi + \dot{\varepsilon}'^{o} \right\rangle - \langle M : B \rangle : \langle B \rangle^{-1} : \langle \Phi \rangle \tag{10}$$

$$\overline{K} = \frac{1-\phi}{\Psi_v}\frac{1-\Psi_g}{\phi}\overline{K} \tag{11}$$

where <.> indicates spatial average. The localization tensors are functions of the local and macroscopic moduli, i.e.: $B = \left(M + \tilde{M}\right)^{-1} : \left(\overline{M} + \tilde{M}\right)$ and $\Phi = \left(M + \tilde{M}\right)^{-1} : \left(\dot{\varepsilon}'^{o} - \dot{E}'^{o} + \tilde{\beta}\right)$; Ψ_g and Ψ_v are the Eshelby factors of grains and voids and ϕ is the porosity. Equations (9-11) are fix-point equations that allow us to obtain improved estimates of the

macroscopic moduli $\overline{M}$, $\dot{E}'^{o}$ and $\overline{K}$. Once $\overline{K}$ is adjusted, the macroscopic dilatation-rate is given by: $\dot{E}_{kk} = P / \overline{K}$ and the porosity-rate can be calculated by means of the well-known kinematic relation:

$$\dot{\phi} = (1-\phi)\,\dot{E}_{kk} \tag{12}$$

The deviatoric local constitutive behavior (1) can be linearized in different ways. The macroscopic response resulting of the selfconsistent formulation will eventually depend on the choice made for that local linearization. For instance, if the back-extrapolated term $\dot{\varepsilon}'^{o}_{ij}$ is a priori set to zero, the resulting model is a secant one, which has been proved to be in general too stiff, leading to close-to-upper-bound result. On the other hand, taking $M_{ijkl} = \partial \dot{\varepsilon}'_{ij}(\sigma') / \partial \sigma'_{kl}$, the resulting model is the so-called affine formulation [5], a less stiff approach. However any homogenization scheme whose local linearization depends only on the average of local states in the phases (or grains) fails in reproducing Gurson's results at high triaxialities, leading to completely rigid response in the pure hydrostatic limit. This result is connected to the high deformation gradients that physically appear inside the phases (or grains), in the vicinities of a void, when high hydrostatic pressure is applied to the aggregate. These strong gradients make the effective response of the phases (or grains) softer than the one that would be obtained by linearization using just the average local states (first order moments).

There are different ways of avoiding this unrealistic rigid response. One procedure consists in using a supertangent formulation [3,4] by defining the local compliance as the one that fulfills:

$$M_{ijkl}\left(\hat{\sigma}'_{kl} - \sigma'_{kl}\right) = \left(\hat{\dot{\varepsilon}}'_{ij} - \dot{\varepsilon}'_{ij}\right) \tag{13}$$

where:

$$\hat{\sigma}'_{kl} = \left(1 + \alpha(\phi, X)X\right)\sigma'_{kl} \tag{14}$$

where $X = P / \Sigma_{eq}$ and $\alpha(\phi, X)$ is a parameter that should be fitted so that the VPSC results match with Gurson's, in the limit of rate-independent isotropic media and spherical voids. The results shown in next section were obtained by means of this Gurson-based fitting procedure.

A more formal way of dealing with the effect of high triaxialities and porosities consists in extending a recently proposed second-order variational method [6] to compressible polycrystals. This method, originally formulated for incompressible materials, makes use of the SC approximation for a linear thermoelastic polycrystal to generate more accurate SC estimates for viscoplastic polycrystals taking into account not only the mean values (first-order moments) but also the average field fluctuations (second-order moments) of the mechanical fields in the grains. This extension of the second-order SC model to compressible polycrystals is currently under development and won't be discussed further here.

RESULTS

Effect of rate-sensitivity

A characteristic of the present formulation is that its results depend on the rate-sensitivity of the material. This feature can be easily visualized by plotting normalized equal-dissipation-rate surfaces, corresponding to different rate-sensitivity exponents. Figure 1 shows these surfaces for 0.5%, 1% and 5% porosity, calculated with VPSC for a random polycrystal with spherical voids, using rate-sensitivity exponents n=1, n=3, n=5 and n=20.

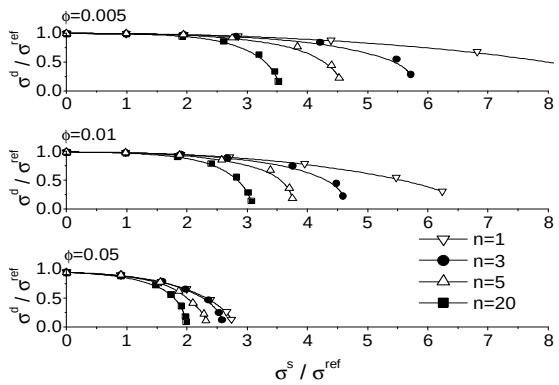

FIGURE 1. Effect of rate-sensitivity. Normalized equal-dissipation-rate surfaces, for porosities 0.5%, 1% and 5%, calculated with VPSC for a random fcc polycrystal with spherical voids, for different rate-sensitivity exponents.

If one assumes that the normal to an equal-dissipation-surface is a reasonable estimate of the strain-rate, it can be seen that: a) as porosity increases, the relative difference between the surfaces corresponding to different rate-sensitivities decreases. In other words, the material becomes less rate-

sensitive as porosity increases, since the cavities themselves are, essentially, rate-insensitive domains; b) at a given porosity and for a fixed stress triaxiality (straight line through the origin), higher rate-sensitivities (lower exponent) give smaller dilatation components and, as a consequence, lower strain triaxialities. Another way of visualizing this effect is displayed in Fig. 2 that shows the porosity evolution of a random fcc polycrystal with 1% initial volume fraction of spherical voids, for different values of the rate-sensitivity exponent and a fixed triaxiality X=1. Evidently, the present model predicts a faster porosity evolution as the rate-sensitivity of the solid material decreases.

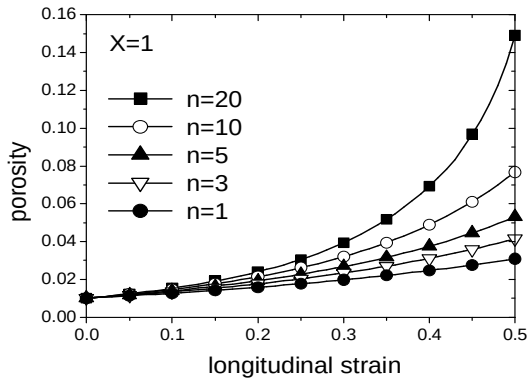

FIGURE 2. Effect of rate-sensitivity on porosity evolution, for a random polycrystal with spherical voids, deforming in tension, for X=1 and different rate-sensitivity exponents. Initial porosity: 1%. Total longitudinal strain: 0.5.

Effect of void morphology

In order to isolate the effects of void morphology from the full anisotropy evolution due to morphologic and crystallographic texture development, we show here results from simulations where neither texture development nor void morphology evolution were allowed. Figure 3 shows the VPSC predictions of porosity evolution during a uniaxial creep test (X=1/3), for a random fcc polycrystal with different void shapes (spherical, oblate and prolate). In the oblate (prolate) case, the short (long) axis of the ellipsoidal void is aligned with the tensile axis. In all cases the rate-sensitivity exponent is n=10, initial porosity is 0.5%, and the total longitudinal strain imposed is 0.5. Oblate voids (axes ratios 5:5:1) tend to grow significantly faster than prolate ones (axes ratios 1:1:5), independent of the triaxiality. This intuitively correct result has also been reported by other authors, using different approaches (e.g.: [7]). Under the present model, the void morphology enters naturally into the formulation via the Eshelby tensor, whose components depend on the orientation and the shape of the cavities present in the material. In addition, it is possible to treat both, aligned or arbitrarily distributed void shapes.

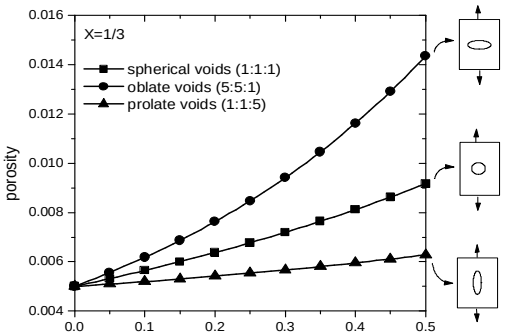

FIGURE 3. Effect of void shape. VPSC predictions of porosity evolution during a creep test performed on an fcc polycrystal with random texture, for different void morphologies, with no texture or morphology evolution. Initial porosity: 0.5%, n=10, total longitudinal strain: 0.5.

Comparison with unit cell FE model

At this point, it is interesting to compare the results of the present theory with those of a Finite Element calculation of a porous viscoplastic unit cell. Figure 4 shows relative porosity (ϕ/ϕ_o), void aspect-ratio and longitudinal strain, as functions of time, during a creep test, as predicted with VPSC and the corresponding FE results, reported by Garajeu et al. [8]. In both simulations, the initial porosity ϕ_o is 0.1%, the void shape is initially spherical and the rate-sensitivity exponent is n=5. Cases for two different triaxialities (X=0.762 and X=1.833) are compared. At a lower triaxiality, VPSC slightly overestimates porosity evolution while, at a higher triaxiality, porosity evolution and, consequently, longitudinal strain are underestimated by VPSC. Moreover, for both triaxilities considered here, VPSC overestimates the void aspect-ratio evolution, with respect to FE results. The underestimation of porosity evolution (and, consequently, of longitudinal strain) at high triaxialities (i.e.: when the volume fraction of voids undergoes a rapid increase) can be ascribed to the lack of void interaction, implicit in the VPSC formulation.

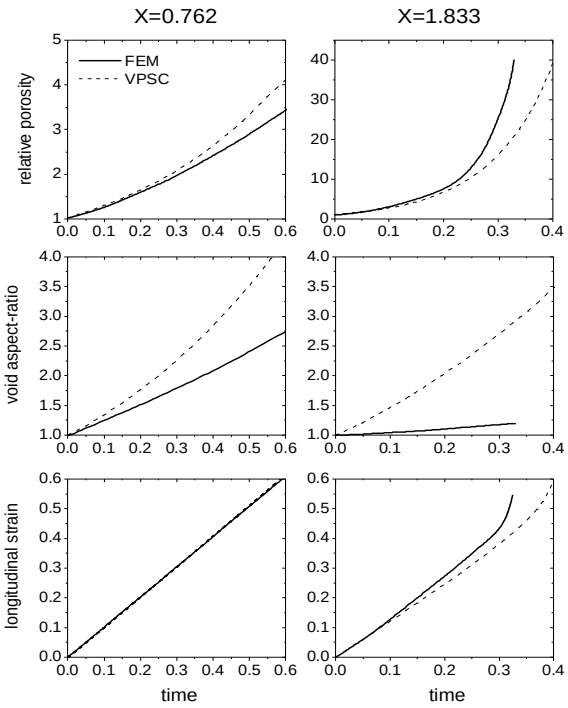

FIGURE 4. Comparison with unit cell FE results. Finite Element predictions for a 3D porous viscoplastic unit cell (after Garajeu et al. [8]) vs. VPSC predictions of: relative porosity, void aspect-ratio and longitudinal strain as function of time. Initial porosity: 0.1%; initial void shape: spherical; rate-sensitivity: n=5.

Coupling between texture and porosity evolution

The present model allows us to account for the anisotropic response of voided polycrystals induced by the development of crystallographic and/or morphologic texture. While the former is due to crystal rotations associated with plastic distortion of the grains, the latter refers to changes in the shape of both, voids and grains. The anisotropy induced by texture development in a polycrystal with initial random texture gradually affects the porosity evolution. As a consequence, it is to be expected that a simulation carried out in an initially textured polycrystal along different directions should predict a different trend of void growth, from the very beginning of the deformation. Furthermore, this anisotropic behavior should be more marked if the plastic anisotropy of the single crystal is higher. For this reason, the next example concerns texture and porosity evolution simulations carried on an hcp material, with easy $(0001)<1\bar{2}10>$ basal and $(10\bar{1}0)<1\bar{2}10>$ prismatic <a> slip and four times harder $(10\bar{1}1)<11\bar{2}3>$ pyramidal <c+a> slip and an initial texture consisting of a strong basal component along the axis x_1 (Fig. 5c, left). The imposed stress states were axisymmetric, with the tensile axis parallel to x_1 or parallel to x_2, with a constant axial strain-rate of 1 s^{-1} and constant lateral stresses chosen to give an initial triaxiality of 1. The initial porosity was 1% of spherical voids and the final longitudinal strain was 0.5. Other conditions of these simulations were: n=10, texture and morphology evolution allowed, and no mechanical strain-hardening (i.e.: constant threshold stresses for every slip system throughout deformation). Figure 5 shows: a) the predicted stress-strain curves (including analogous cases without voids), b) the triaxiality and porosity evolution and c) the initial and final textures. It can be seen that the texture evolution depends on the orientation of the tensile axis relative to the initial texture (Fig. 5c) and, that the porosity evolution is also strongly influenced by the direction of loading, relative to the texture (Fig. 5b). Indeed, the case of tension along x_1 (i.e.: most crystals with their <c>-axis aligned in tensile direction and therefore hard to deform) exhibits a faster void growth than the case of tension along x_2. The reason for this is that the material chooses to accommodate deformation by opening the voids, rather than by deforming plastically along the hard direction. The coupling between the hydrostatic component and the material plastic anisotropy is strong: the hydrostatic component leverages the latter mechanism, and promotes the void contribution to deformation. The response of this hcp aggregate provides a dramatic example of a case where the combined anisotropy of the single crystal and of the polycrystal (texture) affect the evolution of porosity substantially. The difference in porosity evolution predicted above when the textured hcp plate is made to deform in tension along different directions, should also manifest itself in the overall mechanical response. Note that, unlike a creep test simulation, these mixed boundary conditions determine changes in triaxiality (an increase, in these cases) as deformation proceeds (Fig. 5b). The stress-strain curves (Fig. 5a) without porosity show a geometric softening consistent with the texture evolution shown in Fig. 5c. Furthermore, if the textured plate is initially voided and porosity evolution is allowed, in the case of tension along x_1 a fast porosity evolution induces a significant additional softening (and, consequently, a marked increase of the triaxiality), while, in the case of tension along x_2, the contribution to softening of the slow porosity evolution is only marginal.

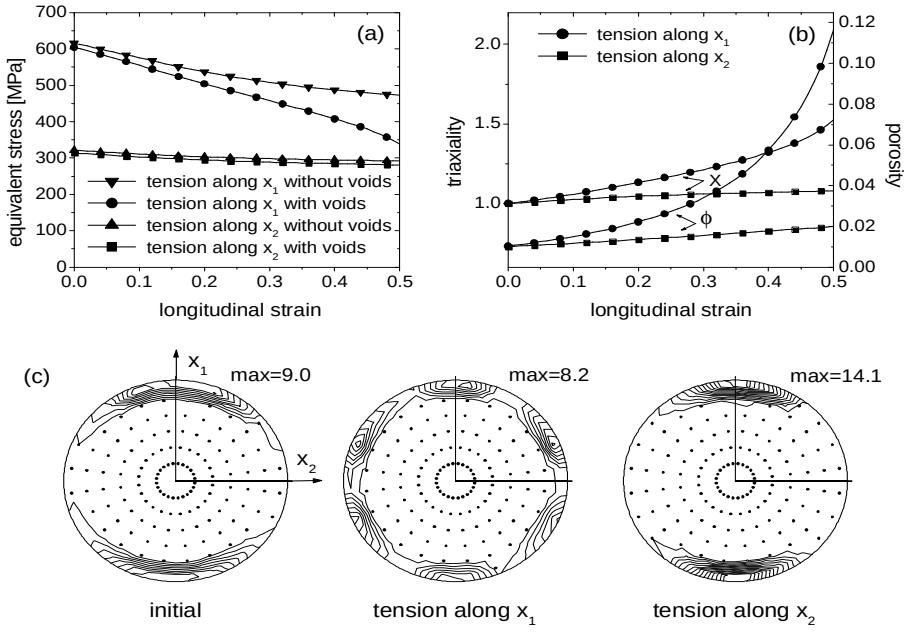

FIGURE 5. VPSC predictions of (a) stress-strain curves for a textured hcp polycrystal, deformed in tension along x_1 and x_2, at a constant longitudinal strain-rate of 1 s^{-1} and an initial triaxiality of 1. Cases with and without porosity. (b) corresponding porosity (right axis) and triaxiality (left axis) evolution. (c) initial and final (0001) basal poles figures. Initial porosity: 1%, n=10, prismatic and basal slip (τ^s =100 MPa) and pyramidal <c+a> slip (τ^s =400 MPa). Total longitudinal strain: 0.5.

CONCLUSIONS AND FUTURE WORK

The earlier incompressible version of VPSC has been interfaced with FEM to perform multiscale calculations where the former was used to get the constitutive response of each material point, inside larger plastic forming codes [9]. Likewise, the present compressible VPSC can be used as a constitutive routine inside dynamic FE codes, for the simulation of high strain-rate deformation processes in which both anisotropy and cavitation become relevant aspects of microstructural evolution. In doing this, a polycrystalline aggregate should be associated with each FE integration point. The VPSC-FE code should impose the computed velocity gradient on each of these polycrystals, then update the shape, orientation and hardening of the individual grains, as well as the shape and volume fraction of voids, depending on the deformation history of the element, and finally get the macroscopic stress for use in the solution of the continuum equilibrium equations. This compressible VPSC-dynamic FE coupling is presently in progress.

REFERENCES

1. Gurson A.L. *J. Eng. Mater. Technol*. **99**, 2-15 (1977).
2. Lebensohn R.A. and Tomé C.N. *Acta metall. mater*. **41**, 2611-2624 (1993).
3. Lebensohn R.A., Maudlin P.J. and Tomé C.N. *LANL Internal Report* LA-UR-03-1193, ***http://www.lanl.gov/mst/voids.shtml,*** 2003.
4. Lebensohn R.A., Maudlin P.J. and Tomé C.N. *J. Mech. Phys. Solids* **52**, 249-258 (2004).
5. Masson R., Bornert M., Suquet P. and Zaoui A. *J. Mech. Phys. Solids* **48**, 1203-1227 (2000).
6. Ponte Castañeda P. *J. Mech. Phys. Solids* **50**, 737-757 (2002).
7. Lee B.J. and Mear M.E. *J. Mech. Phys. Solids* **39**, 45-71 (1991).
8. Garajeu M, Michel J.C. and Suquet P. *Comput. Methods in Appl. Mech. Engrg.***183**, 223-246 (2000).
9. Tomé C.N., Maudlin P.J., Lebensohn R.A. and Kaschner G.A., *Acta mater* **49**, 3085-3096 (2001).